

# Molecular Design of UV–vis Absorption and Emission Properties in Organic Fluorophores: Toward Larger Bathochromic Shifts, Enhanced Molar Extinction Coefficients, and Greater Stokes Shifts

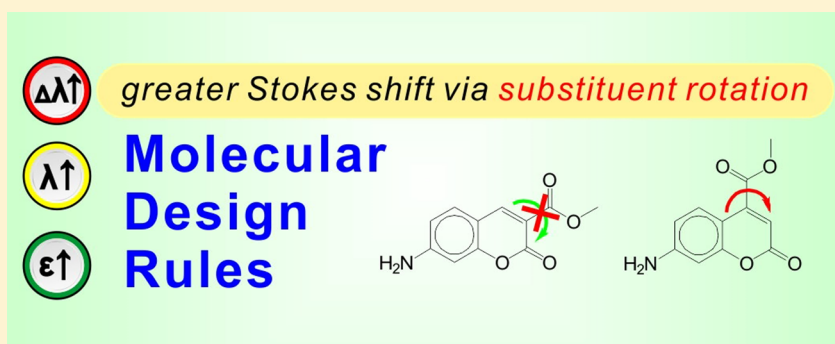
Xiaogang Liu,<sup>†</sup> Zhaochao Xu,<sup>\*,‡</sup> and Jacqueline M. Cole<sup>\*,†,§,||</sup>

<sup>†</sup>Cavendish Laboratory, Department of Physics, University of Cambridge, J. J. Thomson Avenue, Cambridge CB3 0HE, U.K.

<sup>‡</sup>Dalian Institute of Chemical Physics, Chinese Academy of Sciences, Dalian 116023, China

<sup>§</sup>Department of Chemistry, University of New Brunswick, P.O. Box 4400, Fredericton, NB, E3B 5A3, Canada

<sup>||</sup>Department of Physics, University of New Brunswick, P.O. Box 4400, Fredericton, NB, E3B 5A3, Canada



**ABSTRACT:** Understanding the molecular origins of the optoelectronic properties of fluorophores provides rational guidelines for chemists to synthesize better-performing dyes. Factors affecting the UV–vis absorption spectral shift, molar extinction coefficients, and Stokes shift of fluorophores are herein examined at the molecular level, via both (time-dependent) density functional theory-based calculations and the empirical harmonic-oscillator-stabilization-energy (HOSE) and bond-length-alternation (BLA) models. The importance of these factors is discussed using six coumarin dyes as exemplars. In particular, a special focus is devoted to the Stokes shift, a critical parameter in fluorophores. It is demonstrated that incorporating a “rotational” substituent in a fluorophore molecule with tailored steric hindrance effects and resonance effects leads to a substantial increase in the Stokes shift, not only in coumarins but also in other chemical dye families: boron-dipyrromethenes (BODIPYs), cyanines, and stilbenes. Structure–property relationships concerning the rotational substituent are discussed in detail with examples of several dye families. These findings lead to the proposal of molecular design criteria that enable one to tune the Stokes shift. Such criteria provide a foundation for the molecular engineering of fluorophores with improved optoelectronic properties.

## 1. INTRODUCTION

Fluorophores have been used extensively in a wide range of applications, such as biomolecular labels, chemical sensors, cellular stains for chemical biology research,<sup>1–4</sup> and medical diagnosis.<sup>5–7</sup> They have also been deployed in organic light emitting diodes as display devices<sup>8</sup> and sensitizers for dye-sensitized solar cells.<sup>9,10</sup> Fluorophores are mainly characterized by their UV–vis absorption and fluorescence spectra, molar extinction coefficients, quantum efficiencies, and Stokes shifts.<sup>1</sup> Tuning their spectra allows one to choose an appropriate excitation and emission wavelength, at which the background absorption or scattering is minimized and the penetration of the signal light is maximized.<sup>11</sup> A large molar extinction coefficient coupled with a high quantum efficiency is preferred, as their product corresponds to the fluorescence brightness.<sup>1</sup> In addition, a large Stokes shift helps to minimize the self-quenching effect; a greater separation of the excitation and

emission wavelengths also boosts the signal-to-noise ratio in bioimaging applications.<sup>12</sup>

However, few fluorophores have optimal performance in all of these aspects, thus withholding them from widespread applications. For example, the Stokes shifts of most rhodamine<sup>13</sup> and boron-dipyrromethene (BODIPY) dyes<sup>14–16</sup> are typically limited to only ~20 nm.<sup>1</sup> Consequently, the materials discovery of new dyes with improved photophysical and photochemical properties is still of considerable interest. One approach to develop new dyes is to invent new fluorophore scaffolds. This approach can be further classified into two pathways. One pathway is to design entirely new dye frameworks, such as Qian’s dyes,<sup>17</sup> GFP-chromophore

Received: April 27, 2013

Revised: July 4, 2013

Published: July 17, 2013



analogues,<sup>18</sup> difluoroboroazaobenzazulene dye,<sup>19</sup> and “Seoul-Fluor” dyes;<sup>20,21</sup> the other is a hybrid pathway where two or more existing types of fluorophores are combined into a single molecule, such as the “Changsha” dyes,<sup>22</sup> which are essentially composed of a rhodamine dye and part of a cyanine dye. Nevertheless, developing new fluorophore scaffolds remains a very challenging task. To date, the oft-used dyes in biochemical research are still limited to a few chemical families, such as rhodamine, BODIPY and coumarin derivatives.<sup>1,23,24</sup> Moreover, the biocompatibility, photophysics, and photochemistry of new dye families require more extensive studies before their deployment on a large scale. In contrast, an easier and more promising approach is to attach different chemical substituents into the molecular frameworks of the few well-known families of fluorophores to fine-tune their properties since there are many individual dyes available within these few families from which researchers can select.<sup>1</sup> The introduction of combinatorial chemistry has sped up this process by efficient synthesis of a large number of candidate compounds, from which satisfactory dyes can be screened.<sup>25–28</sup>

Unfortunately, only some general guidelines are considered for the design of new dyes at the present time. For example, increasing the “push–pull” effect in dyes, whose excitation involves intramolecular charge transfer (ICT), results in a red shift in their UV–vis absorption and emission spectra; expanding their  $\pi$ -conjugated network also leads to a bathochromic shift and an enhanced molar extinction coefficient; and enlarging the geometrical relaxation when the molecule exists in its excited state boosts the Stokes shift of a dye. However, prior to chemical synthesis, one may not be sure which position to attach a substituent in the dye framework to maximize the spectral shift. An even more puzzling question concerns the Stokes shift: although it has been suggested that the rotation of a molecular structure upon its excitation leads to a large Stokes shift, such as in biphenyl,<sup>29</sup> 9-*t*-butylanthracene,<sup>30</sup> pyrazolo-coumarin derivatives,<sup>30</sup> heptamethine cyanine dyes,<sup>31</sup> and BODIPY dyes,<sup>32</sup> there is a lack of detailed guidelines on how to design new fluorophores with such rotating structures and large Stokes shifts; moreover, introducing substituents to a fluorophore framework often shifts the UV–vis absorption and emission spectra of the dye in the same direction. Consequently, the overall change in the Stokes shift remains small. It is also worth mentioning that other strategies to increase the Stokes shifts suffer from their own problems: for example, the Förster resonance energy transfer does not completely eliminate self-absorption and inner-filter effects,<sup>12</sup> and not all dyes are capable of forming excimers upon their excitation.

As a result, the development of new fluorophores is still largely based on trial-and-error. The typical approach of adding chemical substituents to the dye framework does not necessarily lead to better-performing fluorophores but often produces unnecessarily complicated compounds. In contrast, small fluorophore molecules are often preferred, as they are generally easier to synthesize, and their smaller volumes allow them to access tiny cavities, i.e., to reach certain protein targets or semiconductor interfaces, thus becoming more useful. Two critical questions are thus raised: (1) given a fluorophore core molecular framework and a chemical substituent, can one *substantially* modify dye properties by changing the substituent position or modifying the molecular geometry, but without introducing additional atoms into the system? (2) If so, what are the fundamental molecular structure–property relationships

that lead to a judicious strategy, and can such a strategy be translational to different dye families?

In this paper, we will address these two questions by revealing the relevant structure–property relationships of organic dyes at the molecular level. Coumarins are used as examples to demonstrate that the substituent positional effect affords considerable impact on the UV–vis absorption spectra, the molar extinction coefficients, and the Stokes shifts of fluorophores. To this end, (time-dependent) density functional theory (DFT/TD-DFT) calculations, the empirical harmonic-oscillator-stabilization-energy (HOSE) model,<sup>33</sup> and bond-length-alternation (BLA) analysis<sup>34–36</sup> are employed, with a special focus on the increase in the Stokes shift. It will be shown that a three-dimensional consideration in the molecular structure is critical for understanding the substituent positional effects. In addition, an excursion to the BODIPY dyes, cyanines, and stilbenes is made in the discussion of creating fluorophores with large Stokes shifts, to develop important guidelines on designing a “rotating” fluorophore. The associated molecular origins of these structure–property relationships will provide rational guidelines for experimentalists to design and synthesize new fluorophores with improved optoelectronic properties.

## 2. COMPUTATIONAL DETAILS

Quantum-chemical calculations were performed using Gaussian 09.<sup>37</sup> Becke’s three-parameter and Lee–Yang–Parr hybrid functional (B3LYP)<sup>38–40</sup> and a 6-31+G(d,p) basis set<sup>41</sup> were used for the geometry optimizations of coumarins in both their ground and first excited states, in ethanol solution as accounted for via the polarizable continuum model (PCM).<sup>42,43</sup> Following this, TD-DFT calculations were carried out on the optimized ground-state molecular structures to determine their peak absorption wavelengths and molar extinction coefficients, with the CAM-B3LYP functional<sup>44</sup> and 6-31+G(d,p) basis set.

B3LYP/6-31G(d) was employed in the gas-phase calculations of the other dyes: BODIPY, cyanines, and stilbenes, to reduce the computational load.

In all calculations, frequency checks were performed after each geometry optimization to ensure that minima on the potential energy surfaces were found.

## 3. RESULTS AND DISCUSSION

**3.1. Establishing Structure–Property Relationships in Coumarin Dyes.** A schematic drawing of the parent coumarin framework (2H-chromen-2-one; **1**), together with its position-numbering convention and the atomic labeling used in this paper, is shown in Figure 1. In addition, we define the aromatic ring consisting of 6 carbon atoms as Ring 1 and the lactone ring as Ring 2.

Among many commercially available coumarins, a popular design strategy is to attach one electron-donating substituent at the 7-position and another electron-withdrawing or -donating group at either the 3-position or 4-position, such as in **2–8** (Scheme 1). This strategy can effectively adjust the “push–pull” effect and shift the UV–vis spectra of coumarins, by simply changing substituents according to their varying electron-donating or -withdrawing power.<sup>45,46</sup> Henceforth, we also define coumarins with Ring 2 substituents at the 3-position as the set {3-sub}; similarly, {4-sub} represents coumarins with substituents at the 4-position.

In previous work, we demonstrated that attaching an electron-withdrawing group at the 3-position instead of the 4-

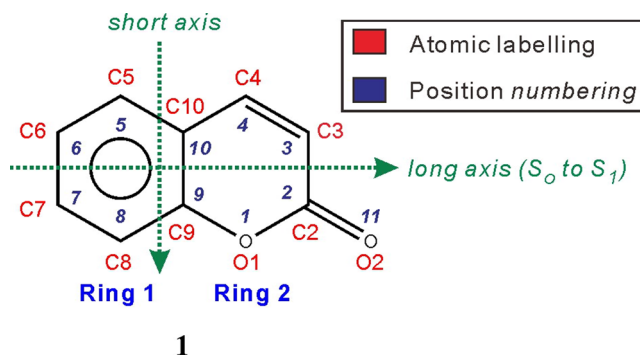


**Figure 1.** Molecular structure of coumarin and its atomic and ring labeling and position numbering designations.

position leads to a larger red shift in the UV–vis absorption spectra and an almost doubled molar extinction coefficient.<sup>46,47</sup> However, in those studies, the {3-sub} and {4-sub} coumarins carry different chemical substituents. To gain a deeper understanding of the substituent positional effect, a natural option is to use the same substituent but attach it at different positions in the coumarin framework and then compare the optoelectronic properties of the resulting compounds. For instance, it is found that a 3-position-substituted coumarin, **8a**, has a longer peak absorption wavelength ( $\lambda_{\text{max}}^{\text{abs}}$ ) but shorter peak fluorescence wavelength ( $\lambda_{\text{max}}^{\text{flu}}$ ), as well as larger molar extinction coefficient ( $\epsilon$ ) at its  $\lambda_{\text{max}}^{\text{abs}}$  relative to the 4-position-substituted coumarin, **8b** (Scheme 1; Table 1). The most striking difference between **8a** and **8b** is probably the substantially different Stokes shifts: 43 and 102 nm, respectively (Table 1). To verify whether these patterns are a coincidence, we performed an extensive literature search and found seven 3/4-substitution pairs of coumarin compounds, each with exactly the same substituent, but attached at different positions (Scheme 1). The optoelectronic properties of these compounds have been determined previously, and their optoelectronic properties share exactly the same pattern as those of **8a** and **8b** (Table 1). This suggested a fundamental rationale beneath our observations. Accordingly, due comprehension was sought by developing new structure–property relationships concerning the substituent positional effect. Given the importance of preventing electron quenching in so many applications of fluorophores, special attention was given to understanding the molecular origins of large Stokes shifts.

DFT and TD-DFT calculations were employed to assist in the analysis of the structure–property relationships. It has been demonstrated that the theoretically optimized molecular structures based on DFT calculations bear good agreement with the experimental derived data using X-ray diffraction.<sup>47,48</sup> TD-DFT has also been shown to be a powerful tool to model the spectroscopic properties of organic fluorophores.<sup>49,50</sup> In addition, empirical HOSE and BLA models, which successfully correlate the structural features of coumarins to their optoelectronic properties,<sup>47,51</sup> are applied in this study as well.

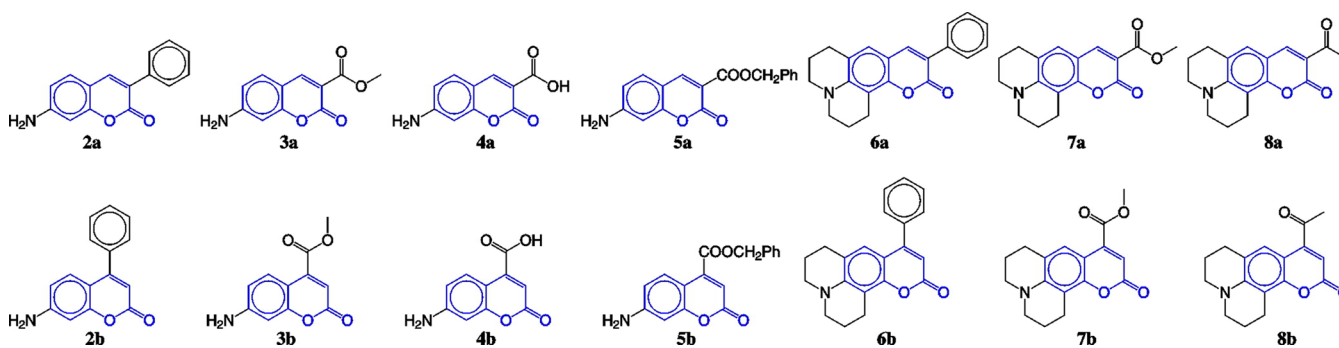
**3.1.1. Structure–Property Relationships for the UV–vis Absorption Spectra.** Before considering the substituent positional effect on the UV–vis absorption spectra of 2–8, two reference coumarins, **9** and **10**, with only hydrogen atoms at the 3- and 4-positions, need to be analyzed (Scheme 2).

The first excited states of **9** and **10** involve predominantly the HOMO  $\rightarrow$  LUMO electron transition. The atomic contributions to their HOMO and LUMO electron densities are thus computed via DFT (Figure 2). At the 4-position, the electron density is very low in the HOMO but increases considerably in the LUMO for both **9** and **10**. Therefore, attaching an electron-withdrawing group at the 4-position will greatly stabilize the LUMO and reduce the energy bandgap of a coumarin.<sup>59</sup> In contrast, the electron density at the 3-position bears little change during the HOMO  $\rightarrow$  LUMO transition. Accordingly, an electron-withdrawing group attached at this position causes similar stabilization effects to both the HOMO and the LUMO, and the overall change in the energy bandgap should be relatively small.

The above analysis, employed in many studies to facilitate the design of new fluorophores,<sup>20,21,59</sup> suggests that attaching an electron-withdrawing group at the 4-position causes a smaller bandgap in coumarins. This prediction, however, is obviously different from our early observation by experiment, that the {3-sub} coumarins exhibit larger red shifts relative to the {4-sub} (Table 1).<sup>46</sup> The simple analysis of electron density changes during the HOMO  $\rightarrow$  LUMO transition on reference coumarins clearly cannot resolve these contradictory results. A more in-depth structure–property relationship investigation is thus required.

The bandgap ( $E_g$ ) of a compound is determined predominantly by five factors (eq 1).<sup>60</sup> The first factor ( $E_{\text{sub}}$ ) involves the electron-donating/-withdrawing power of a substituent, which is often quantified by Hammett values.<sup>61</sup> This factor plays an important role in the spectral shift of a

**Scheme 1.** Molecular Structures of 14 Coumarin Derivatives (2–8)<sup>a</sup>



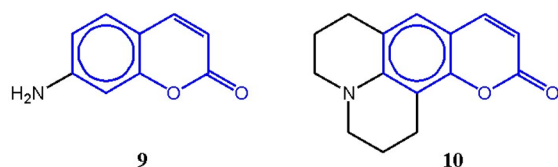
<sup>a</sup>The common coumarin fragment is highlighted in blue. Each pair (one from the top row and the other from the bottom row) of these coumarins has the same substituent, but attached at different positions, i.e., at the 3-position and the 4-position, respectively.

**Table 1.** Experimental Spectral Intensity Maxima of UV–vis Absorption and Fluorescence [ $\lambda$  (nm) and  $\nu$  ( $\text{cm}^{-1}$ )], Stokes Shifts [ $\Delta\lambda$  (nm) and  $\Delta\nu$  ( $\text{cm}^{-1}$ )], and Molar Extinction Coefficients at the Peak Absorption Wavelengths [ $\epsilon$  ( $\times 10^4 \text{ L cm}^{-1} \text{ mol}^{-1}$ )] of 2–8<sup>a</sup>

|                  | {3-sub}                             |                    |                                     |                    |                 |             |                                     | {4-sub}            |                    |                                     |                    |                 |              |            |      |
|------------------|-------------------------------------|--------------------|-------------------------------------|--------------------|-----------------|-------------|-------------------------------------|--------------------|--------------------|-------------------------------------|--------------------|-----------------|--------------|------------|------|
|                  | absorption                          |                    | fluorescence                        |                    | Stokes shift    |             |                                     | $\epsilon$         | absorption         |                                     | fluorescence       |                 | Stokes shift |            |      |
|                  | $\lambda_{\text{max}}^{\text{abs}}$ | $\nu_{\text{abs}}$ | $\lambda_{\text{max}}^{\text{flu}}$ | $\nu_{\text{flu}}$ | $\Delta\lambda$ | $\Delta\nu$ | $\lambda_{\text{max}}^{\text{abs}}$ |                    | $\nu_{\text{abs}}$ | $\lambda_{\text{max}}^{\text{flu}}$ | $\nu_{\text{flu}}$ | $\Delta\lambda$ | $\Delta\nu$  | $\epsilon$ |      |
| 2a <sup>52</sup> | 378                                 | 26455              | -                                   | -                  | -               | -           | 2.70                                | 2b <sup>53,b</sup> | 364                | 27473                               | 491                | 20367           | 127          | 7106       | 1.55 |
| 3a <sup>54</sup> | 399                                 | 25063              | 442                                 | 22624              | 43              | 2438        | 1.07                                | 3b <sup>54</sup>   | 383                | 26110                               | 540                | 18519           | 157          | 7591       | 0.69 |
| 4a <sup>54</sup> | 404                                 | 24752              | 445                                 | 22472              | 41              | 2281        | 1.07                                | 4b <sup>54</sup>   | 388                | 25773                               | 494                | 20243           | 106          | 5530       | 0.51 |
| 5a <sup>54</sup> | 401                                 | 24938              | 442                                 | 22624              | 41              | 2313        | 1.62                                | 5b <sup>54</sup>   | 392                | 25510                               | 541                | 18484           | 149          | 7026       | 0.60 |
| 6a               | 415 <sup>55</sup>                   | 24096              | 492 <sup>55</sup>                   | 20325              | 77              | 3771        | 3.25 <sup>56,c</sup>                | 6b <sup>56,d</sup> | 406                | 24631                               | 526                | 19011           | 120          | 5619       | 2.14 |
| 7a               | 436 <sup>57</sup>                   | 22936              | 480 <sup>57</sup>                   | 20833              | 44              | 2102        | 4.68 <sup>e</sup>                   | 7b <sup>54</sup>   | 434                | 23041                               | 575                | 17391           | 141          | 5650       | 0.91 |
| 8a <sup>45</sup> | 452                                 | 22124              | 495                                 | 20202              | 43              | 1922        | 4.90                                | 8b <sup>58</sup>   | 418                | 23923                               | 520                | 19231           | 102          | 4693       | 1.29 |

<sup>a</sup>All data are collected in ethanol, unless stated otherwise. <sup>b</sup>All data of 2b are measured in methanol. <sup>c</sup>The  $\epsilon$  of 6a is measured in 95% aqueous ethanol. <sup>d</sup>All data of 6b are measured in 95% aqueous ethanol. <sup>e</sup>The  $\epsilon$  of 7a is estimated based on the value of coumarin 314, a very similar compound to 7a.<sup>45</sup>

### Scheme 2. Molecular Structures of Two Reference Coumarin Compounds 9 and 10<sup>a</sup>



<sup>a</sup>Their common coumarin fragment is highlighted in blue.

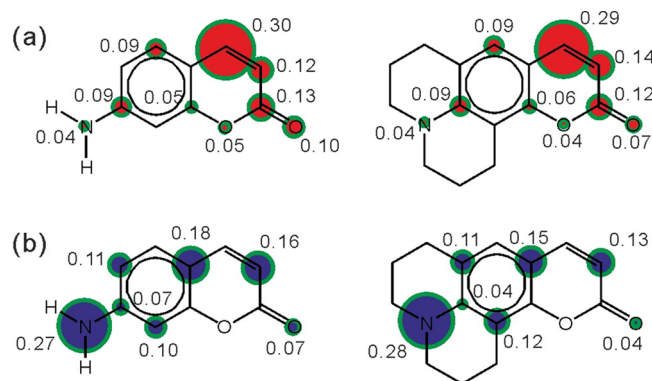
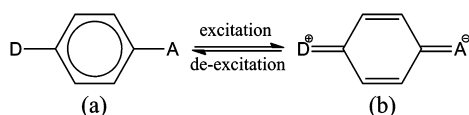


**Figure 2.** Atomic contributions to: (a) LUMO and (b) HOMO electron densities, for 9 (left) and 10 (right). The blue/red circle diameter represents the atomic contribution; only contributions greater than 0.02 are shown.

“push–pull” (donor– $\pi$ -bridge–acceptor) dye (Scheme 3); i.e., an enhanced push–pull effect leads to a larger red shift. The

### Scheme 3. Resonance Structures of a “Push–Pull” Benzenoid Dye



second factor is represented by bond length alternation (BLA).<sup>34–36</sup> BLA calculates the difference of the average single-bond length and average double-bond length in the conjugated alkyl chain of a molecule.<sup>34–36</sup> A smaller BLA value corresponds to a higher degree of electron delocalization and a

smaller bandgap. The third factor ( $E_{\text{res}}$ ) concerns the resonance energy in a ring-type conjugated system. For example, the optical excitation of an aromatic dye [Scheme 3(a)] involves ICT and the switching of its benzene ring to a *para*-quinoidal form [Scheme 3(b)]. Conversely, the resonance energy tends to confine the  $\pi$ -electrons within the benzene ring and works against ICT.<sup>60</sup> The amount of resonance energy can be related to the ground-state molecular structure of an aromatic dye. According to resonance theory, the actual observed molecular structure of a molecule is collectively described by all its possible resonance states. While Scheme 3(a) is more representative of the ground state of the aromatic dye, Scheme 3(b) is another possible resonance state of this compound. Consequently, the observed benzene ring in this dye is not absolutely aromatic. Rather, they display quinoidal-like patterns, due to the contributions for the *para*-quinoidal resonance state 3(b). The contributions from these different resonance states can be quantified by the empirical HOSE model.<sup>33</sup> In particular, the contribution from the *para*-quinoidal resonance state [Scheme 3(b)] to the ground-state structure gives a good indication about the resonance energy; i.e., a higher *para*-quinoidal contribution corresponds to lower resonance energy. The fourth factor can be understood as the dihedral angle,  $\theta$ , between the substituent and the coumarin framework in our case. This is particularly important when this substituent can participate in and extend the  $\pi$ -conjugated network in coumarins. A smaller  $\theta$  results in a more planar structure and a larger  $\pi$ -electron delocalization, causing a smaller  $E_{\theta}$ . The last factor ( $E_{\text{int}}$ ) accounts for intermolecular interactions.<sup>60</sup> In our study, each pair of 3/4-substituted coumarins, which possess the same substituent but attached at different positions, has the same molecular formula and similar volumes, and these coumarins are mainly deployed in the solution phase for various applications. Hence, the contribution from the intermolecular interactions, essentially the solvent–solute interactions, is comparable among each pair. Our discussion will thus focus only on the first four factors. Lastly, it should be pointed out that these five factors do not act separately but are often correlated. For example, increasing the push–pull effect by choosing more electron-donating/-withdrawing substituents tends to decrease  $E_{\text{sub}}$ ; at the same time, the molecular structure of the resulting dye becomes more *para*-quinoidal, affording a lower  $E_{\text{res}}$ .<sup>60</sup>

$$E_{\text{g}} = E_{\text{sub}} + E_{\text{BLA}} + E_{\text{res}} + E_{\theta} + E_{\text{int}} \quad (1)$$

To understand different aspects of the substituent positional effect on  $\lambda_{\text{max}}^{\text{abs}}$ , six representative coumarins, including **2a/b**, **3a/b**, and **8a/b**, are modeled via DFT/TD-DFT. Among these six compounds, **2a**, **3a**, and **8a** belong to set {3-sub}, and their respective analogues **2b**, **3b**, and **8b** are members of the {4-sub} set. The HOSE and BLA analyses and the measurements of dihedral angles ( $\theta$ ) are also performed on the theoretically optimized molecular structures. All results are summarized in Table 2.

**Table 2. Summary of Theoretically-Derived Geometrical Properties of 2a/b, 3a/b, and 8a/b<sup>a</sup>**

|           | {3-sub}        |                       |         | {4-sub}        |          |         |       |
|-----------|----------------|-----------------------|---------|----------------|----------|---------|-------|
|           | $\theta$ (deg) | Q-weight <sup>b</sup> | BLA (Å) | $\theta$ (deg) | Q-weight | BLA (Å) |       |
| <b>2a</b> | 42             | 0.329                 | 0.071   | <b>2b</b>      | 55       | 0.326   | 0.072 |
| <b>3a</b> | 4              | 0.380                 | 0.054   | <b>3b</b>      | 35       | 0.339   | 0.076 |
| <b>8a</b> | 0              | 0.461                 | 0.038   | <b>8b</b>      | 49       | 0.399   | 0.064 |

<sup>a</sup>The geometrical parameters  $\theta$ , Q-weight, and BLA of **2a/b**, **3a/b**, and **8a/b** are calculated based on their theoretically optimized molecular structures in ethanol. <sup>b</sup>Q-weight measures that the contribution of the *para*-quinoidal resonance state among all possible resonance states in Ring 1. This contribution can be quantified by the empirical HOSE model.<sup>33</sup> HOSE describes the energy difference between a particular bond-length pattern in an aromatic ring and the standard Kekulé structure. It is defined as:  $\text{HOSE} = (1)/(2)[\sum_{r=1}^{n_1}(R'_r - R_0^s)^2 k'_r + \sum_{r=1}^{n_2}(R''_r - R_0^d)^2 k''_r]$ , where  $R'_r$  and  $R''_r$  are actual  $\pi$ -bond lengths;  $R_0^s$  and  $R_0^d$  are reference single and double bond lengths;  $n_1$  and  $n_2$  are the number of single and double bonds; and  $k'_r$  and  $k''_r$  are force constants defined as:  $k_r = a + bR_r$ , where  $R_r$  is the actual bond length, and  $a$  and  $b$  are constants derived based on experimental data. For carbon–carbon bonds,  $R_0^s = 1.467$  Å,  $R_0^d = 1.349$  Å,  $a = 44.39 \times 10^4$  Pa, and  $b = -26.02 \times 10^4$  Pa/Å. The HOSE model can be extended to compute the relative contribution for each of the  $n$  resonance states in benzene derivatives.<sup>33</sup> For example, the  $i$ th resonance state has a contribution of:  $C_i = ((\text{HOSE}_i)^{-1})/(\sum_{j=1}^N (\text{HOSE}_j)^{-1})$ . The inverse empirical relationship between the HOSE value of the  $i$ th resonance state and its relative contribution indicates that the more stable resonance state has a larger contribution to the overall molecular structure. Our previous studies have shown the HOSE model to be a useful tool for correlating bond-length patterns to the optical properties of coumarins.<sup>46,47</sup> Details of applying the HOSE model to coumarins can be found in references 46 and 47.

The most noteworthy geometrical difference between the {3-sub} and {4-sub} coumarins lies in the dihedral angle,  $\theta$ . Between each pair of 3/4-substituted coumarins,  $\theta$  is smaller for the {3-sub}. We attribute the smaller  $\theta$  values in {3-sub} to the relatively large “open” space around the 3-position (Figure 3). In contrast, the neighboring atoms around the 4-position are relatively close to the 4-position substituent. When this

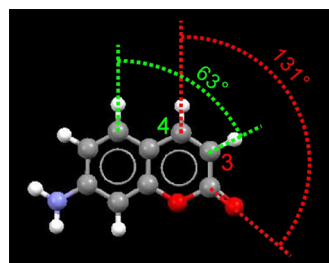


**Figure 3.** Theoretically optimized molecular structure of **9** and a comparison of the “open” space around its 3- and 4-positions.

substituent is bulky, as in the case of **2–8**, the strong steric hindrance effects force this substituent to twist out of the molecular plane of the core coumarin framework.

Owing to the more planar alignment of the 3-position substituents with the coumarin framework plane, these substituents can participate in and extend the  $\pi$ -conjugation network in coumarins more effectively. Consequently, their benzene rings demonstrate a more *para*-quinoidal bond-length pattern, as indicated by their higher Q-weights compared to their {4-sub} analogues. Since Q-weight quantifies the relative contribution of the *para*-quinoidal resonance state [Figure 4(III)], among all possible resonance states, to the actual observed Ring 1 bond lengths, a higher Q-weight corresponds to a lower  $E_{\text{res}}$ . Furthermore, owing to the more effective  $\pi$ -electron delocalization, Ring 2 of {3-sub} also has smaller BLA values than those of the {4-sub} analogues, leading to a lower  $E_{\text{BLA}}$ . For these reasons, the {3-sub} coumarins, including **2a**, **3a**, and **8a**, possess even more red-shifted absorption spectra than their {4-sub} analogues.

Nevertheless, the relative red shift of the UV–vis absorption spectra in {3-sub} with respect to {4-sub} is rather small ( $\sim 15$  nm). Since the errors in TD-DFT calculations are typically of the order of  $\sim 0.2$ – $0.3$  eV,<sup>62</sup> it is not surprising to notice that our TD-DFT calculations qualitatively fail to predict the longer wavelengths of **3a** with respect to **3b** and **8a** with respect to **8b** (Figure 5). The relatively poor accuracy of DFT when dealing with the excitation energies of molecular systems involving BLA and quinoidization has been reported previously.<sup>63–66</sup> The theoretical molar extinction coefficients, on the other hand, agree with experimental data reasonably well.

**3.1.2. Structure–Property Relationships for the Molar Extinction Coefficient.** The unit of the molar extinction coefficient  $\epsilon$  ( $\text{L cm}^{-1} \text{mol}^{-1}$ ) can be simplified into “area/mol”. Intuitively, therefore,  $\epsilon$  is a measure of the “effective” light absorption area per mole of a compound.<sup>67</sup> UV–vis light absorption of coumarins involves ICT. Attaching a substituent along the same direction as the ICT intensifies oscillator strength to a greater degree and leads to a larger increase in the “effective” absorption area.<sup>68</sup>

For a compound with pseudoreflexive symmetry, ICT can occur along either the long or the short molecular axis.<sup>68</sup> In coumarins, electron transfer along the long axis corresponds to a low energy jump ( $S_0$  to  $S_1$ ) compared to that of the short axis ( $S_0$  to  $S_2$ ; Figure 1). {3-sub} coumarins align more closely to the long axis than {4-sub} coumarins. Hence, the impact of the 3-position substituent on  $\epsilon$  is more significant in the first lower energy absorption band than the 4-position substituent that manifests in the second absorption band. Indeed, from the computed UV–vis spectra of 3/4-substituted coumarin pairs (Figure 5), it is clear that {3-sub} coumarins (red) have larger molar extinction coefficients in the first absorption band, while {4-sub} coumarins (blue) absorb more strongly in the second absorption band. It should be noted that the second absorption band is not necessarily dominated by the second excited states. For example, the second peak of **2b** at  $\sim 251$  nm is largely a result of a HOMO-2  $\rightarrow$  LUMO transition (the third excited state).

There is also another, more “quantum”, explanation to the stark difference in molar extinction coefficients between the {3-sub} and the {4-sub}. This discussion will focus only on the first absorption band, which is more relevant to practical applications. However, the same principle can be extended to any absorption band.

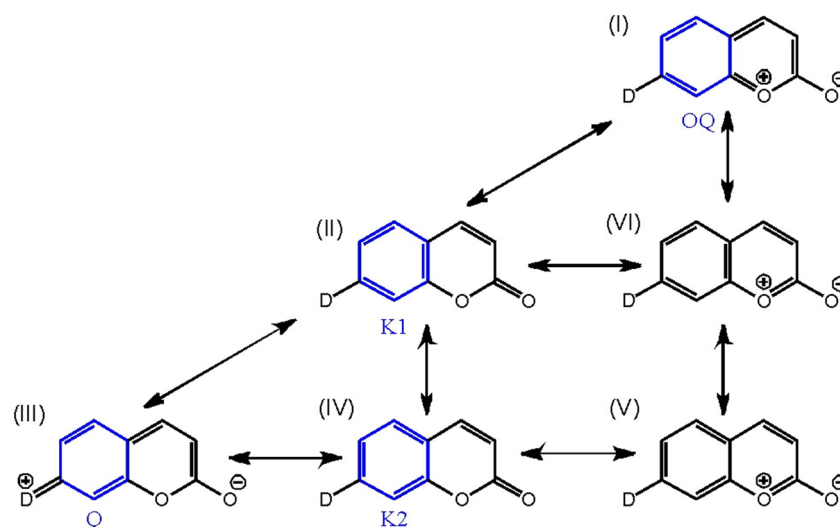


**Figure 4.** Possible resonance structures in coumarin laser dyes. While only the 7-position electron-donating substituent, D, is shown here, other substituents are likely to be attached onto this framework. The blue-highlighted Ring 1 moieties represent four distinct canonical molecular fragments: Q (*para*-quinoidal), OQ (*ortho*-quinoidal), K1 (Kekulé configuration 1), and K2 (Kekulé configuration 2). Their relative contributions toward the DFT-derived molecular structures of Ring 1 can be quantified by the HOSE model (Table 2).

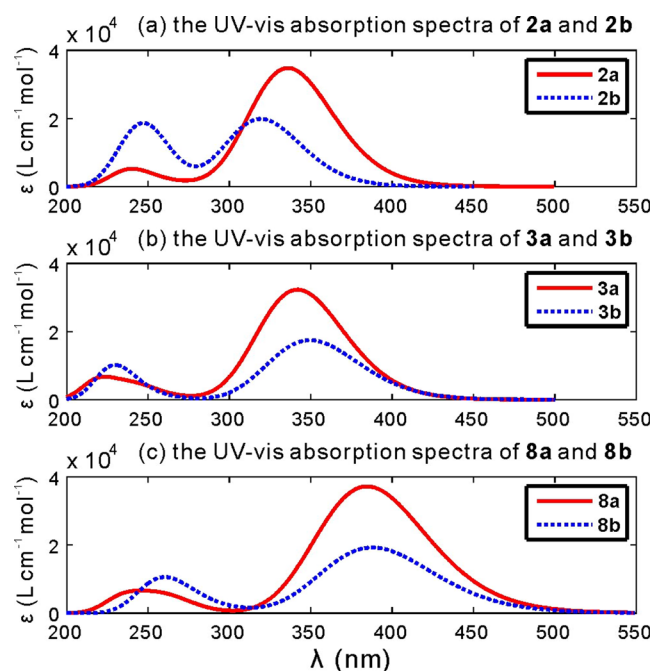


**Figure 5.** Theoretical UV-vis absorption spectra of 2a/b, 3a/b, and 8a/b in ethanol, calculated using TD-DFT with CAM-B3LYP/6-31+G(d,p) and “*nstates* = 8”.

According to quantum mechanics, the light absorptivity of a molecule depends on its transition dipole moment, i.e., a larger transition dipole moment indicates stronger absorptivity. The transition dipole moment measures the coupling between molecular orbitals involved in the light absorption process. For its value to become large, a substantial spatial overlap of electron densities in the involved orbitals is required. In coumarins, the first absorption band is dominated by the HOMO→LUMO transition. Consequently, an examination on the HOMO–LUMO overlap provides useful hints about the transition dipole moments and  $\epsilon$  values.

In the {3-sub} coumarins, the 3-position substituents contribute to both their HOMOs and LUMOs (Figure 6). The overlap between the HOMOs and LUMOs is relatively large in all instances. In contrast, the 4-position substituents have large dihedral angles with respect to the coumarin fragment; they are not actively involved in the HOMOs (Figure 6). Only upon excitation does a substantial amount of charge flow to these substituents in the LUMOs. As a result, the overlap between the HOMOs and the LUMOs in the {4-sub} is relatively small in all cases.

Such overlap can be quantified by an index,  $\Lambda$ .<sup>69</sup> Indeed, for each pair of coumarins with the same substituent (but attached to different positions), we find that the {3-sub} has larger  $\Lambda$  values (Table 3). This observation rationalizes their approximately doubled  $\epsilon$  values, with respect to the {4-sub} coumarins.

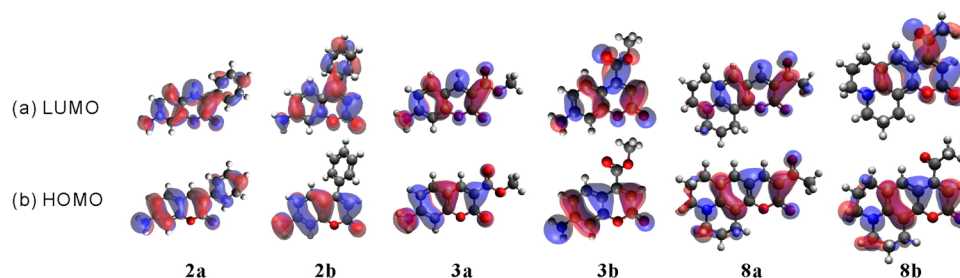


**Figure 6.** Theoretically derived LUMOs and HOMOs of 2, 3, 8–10, and 15 (red: positive; blue: negative; isovalue: 0.02).

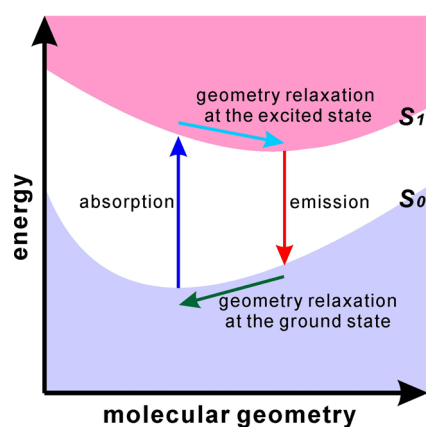
**Table 3.** Summary of Theoretically Derived HOMO–LUMO Overlap Indexes ( $\Lambda$ ) and Geometrical Changes in **2a/b**, **3a/b**, and **8a/b** upon Excitation

|           | {3-sub}     |                                  |                                   |                      |         | {4-sub}   |                                |                                 |                      |         |       |
|-----------|-------------|----------------------------------|-----------------------------------|----------------------|---------|-----------|--------------------------------|---------------------------------|----------------------|---------|-------|
|           | $\Lambda^a$ | $\theta_{\text{ground}}^b$ (deg) | $\theta_{\text{excited}}^c$ (deg) | $\Delta\theta$ (deg) | RMS (Å) | $\Lambda$ | $\theta_{\text{ground}}$ (deg) | $\theta_{\text{excited}}$ (deg) | $\Delta\theta$ (deg) | RMS (Å) |       |
| <b>2a</b> | 0.719       | 42                               | 12                                | 29                   | 0.257   | <b>2b</b> | 0.636                          | 55                              | 26                   | 29      | 0.278 |
| <b>3a</b> | 0.663       | 4                                | 1                                 | 3                    | 0.035   | <b>3b</b> | 0.593                          | 35                              | 0                    | 35      | 0.276 |
| <b>8a</b> | 0.665       | 0                                | 0                                 | 0                    | 0.028   | <b>8b</b> | 0.549                          | 49                              | 2                    | 47      | 0.322 |

<sup>a</sup> $\Lambda$  is an index used to quantify the overlap of HOMO and LUMO in **2a/b**, **3a/b**, and **8a/b**; i.e., a smaller  $\Lambda$  corresponds to less HOMO–LUMO overlap.<sup>69</sup> <sup>b</sup> $\theta_{\text{ground}}$  denotes the dihedral angle between the parent coumarin framework plane and the Ring 2 substituent of a coumarin derivative in its ground-state structure. <sup>c</sup> $\theta_{\text{excited}}$  represents the dihedral angle between the parent coumarin framework plane and the Ring 2 substituent of a coumarin derivative in its first excited state.

**3.1.3. Structure–Property Relationships for the Stokes Shift.** There are substantial differences between the Stokes shifts of the {3-sub} and {4-sub} coumarins. These differences cannot be explained by solvent effects. It is noted that the Stokes shifts of a given coumarin increases by only  $\sim 40$  nm when a nonpolar solvent, such as methyl-cyclohexane or cyclohexane, is swapped for the very polar dimethyl sulfoxide.<sup>70,71</sup> In contrast, changes in the observed Stokes shifts are much larger with an alteration in substituent position. For example, the Stokes shift differences between the 3/4-substituted coumarin pairs are as high as  $\sim 80$  nm, even when compared in the same solvent (Table 1). Therefore, the Stokes shift differences between the 3/4-substituted coumarin pairs are more closely linked to the intrinsic substitutional properties.

The origin of the Stokes shift is illustrated via the modified version of the classical Jablonski diagram (Figure 7).<sup>12</sup>

**Figure 7.** Schematic illustration of the light absorption and emission process in fluorophores.

According to the Franck–Condon principle, UV–vis absorption proceeds via a vertical excitation which is adiabatic; i.e., the absorbed photon energy is not converted into heat; only electrons move, while the nuclei remain stationary. However, the optically excited dye molecule is highly dynamic as it relaxes toward its equilibrium structure accompanied by nuclear motion, and part of the absorbed photon energy is thermalized during this process, before the remaining part re-emits as a photon of a longer wavelength or is completely thermalized via a nonradiative process. To increase the Stokes shift, a large structural change is thus required during the geometry relaxation in the excited state.

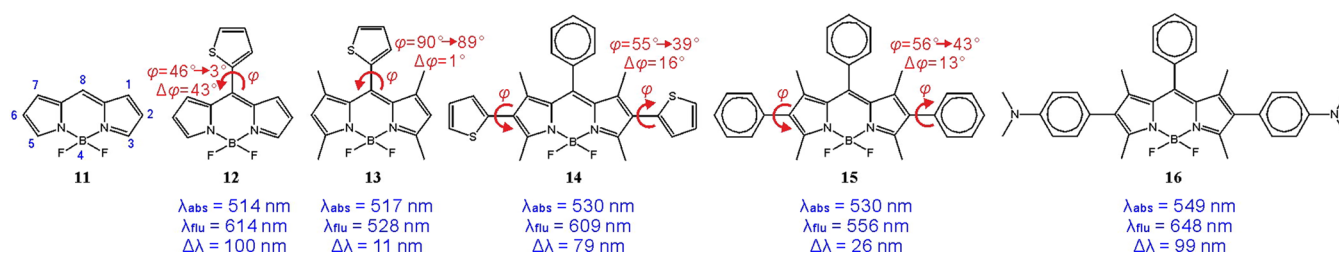
For each pair of 3/4-substituted coumarins that possess the same chemical substituents, it is reasonable to predict that a larger change in the electron density distribution during the

HOMO  $\rightarrow$  LUMO transition (or a smaller overlap between the HOMO and LUMO) will bring about greater nuclear motion during the excited state geometry relaxation. Hence, the HOMO–LUMO overlap index,  $\Lambda$ , provides a good indication of the Stokes shift; i.e., a smaller  $\Lambda$  is correlated to a larger  $\Delta\lambda$  (the Stokes shift in the unit of wavelength) and  $\Delta\nu$  (the Stokes shift in the unit of energy). Indeed, {3-sub} coumarins have smaller  $\Lambda$  values but larger Stokes shifts relative to their {4-sub} analogues (Table 3).

To gain a deeper understanding of photoexcited nuclear motion, we have optimized the molecular structures of **2a/b**, **3a/b**, and **8a/b** in their first excited states using TD-DFT. The most significant geometric changes in the excited state concern the photoexcited rotation of Ring 2 substituents. Once excited, the perturbed wave function (essentially a change in bonding character) causes the Ring 2 substituent to rotate with a tendency to align with the molecular plane of the parent coumarin framework. The dihedral angle,  $\theta$ , is greatly reduced in {4-sub} coumarins (Table 3). In contrast, such rotation is less significant in {3-sub} coumarins, where  $\theta$  values are much smaller, even in the ground state. One exception in the {3-sub} set regards **2a**, which possesses a phenyl ring attached at the 3-position. The phenyl ring is relatively bulky, and even the open space around the 3-position cannot accommodate a planar alignment. Consequently, the  $\theta$  of **2a** is relatively large in the ground state, and its Ring 2 substituent experiences a substantial rotation during excited state geometry relaxation (Table 3).

Molecular structure perturbations occurring during excited state geometry relaxation can also be quantified by taking the root-mean-square (RMS) of the cumulative atomic displacements with respect to the ground-state molecular structures. Indeed, {4-sub} coumarins demonstrate a higher RMS than those of {3-sub}. Their greater photoinduced geometric changes rationalize their larger Stokes shifts (Table 1). For {3-sub} coumarins, the photoinduced geometric changes are generally small, with the exception of **2a**. While experimental Stokes shift data are not available for **2a**, it is interesting to point out that another similar compound, **6a**, also with a phenyl ring attached at its 3-position, has almost twice the level of the Stokes shift as compared to other coumarins in {3-sub}, although this is still less than those of {4-sub} (Table 1).

In these coumarins, the rotating substituent is connected to the main coumarin molecular framework via a single bond. Its rotation during the geometry relaxation of the excited state can be explained by two competing effects. One is the effect of steric hindrance, causing it to bend out of the main fluorophore molecular plane; the other is the resonance effect, rendering a tendency to align with the molecular plane to achieve a better electron delocalization. In the ground state, the former effect

Scheme 4. Molecular Structures of BODIPY Dyes 11–16 and the Position Numbering Designations in the BODIPY Framework (11)<sup>a</sup>

<sup>a</sup>The experimental spectral data are all measured in toluene.<sup>32,76,77</sup> The theoretically derived dihedral angle,  $\varphi$ , of the relevant substituents with respect to the BODIPY core framework plane and the theoretically derived dihedral angle changes upon optical excitation,  $\Delta\varphi$ , were modeled by Chen et al.<sup>32</sup>

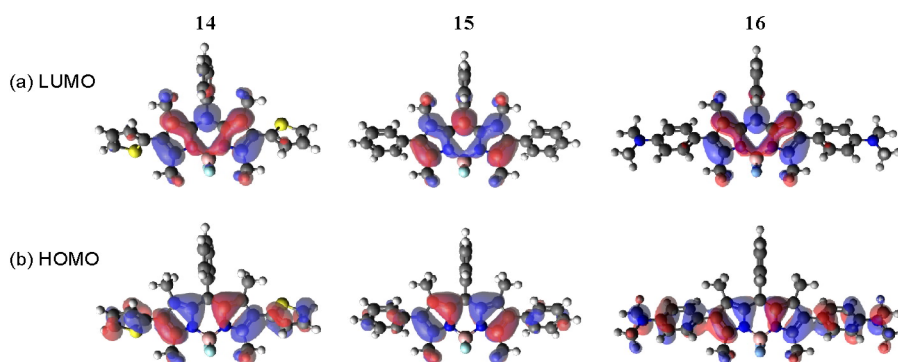


**Figure 8.** Theoretically derived HOMOs and LUMOs of 14 (left), 15 (center), and 16 (right; red, positive; blue, negative; isovalue, 0.02).

dominates, leading to a nonplanar geometry in the resulting fluorophore. Upon excitation, the latter effect gains more strength, driving the substituent to rotate toward a more planar alignment.<sup>72</sup> In other words, the single bond, which connects the substituent and the main fluorophore fragment, displays more double-bonded character upon optical excitation.

Steric hindrance plays an important role in enlarging the Stokes shift. First, this effect causes the substituent to bend out of the main fluorophore plane in the ground state, which creates a prerequisite for this substituent to rotate in the excited state during geometry relaxation. Second, as the substituent rotates in the excited state, a strong interaction between the substituent and its neighboring atoms ensures that a large amount of torsional work is done, which is then translated into the Stokes shift. If steric hindrance is relatively weak, such as in the case of 2a and 6a, a large rotation of the phenyl ring, by 29°, only leads to a relatively modest Stokes shift of ~77 nm (~3700 cm<sup>-1</sup>). In contrast, a similar amount of rotation in 2b and 6b generates a Stokes shift of ~124 nm (~6500 cm<sup>-1</sup>; ~70% increase), owing to the presence of stronger steric hindrance effects.

It should be noted that the rotation of these substituents upon their optical excitation is very different from twisted intramolecular charge transfer (TICT).<sup>73,74</sup> In TICT, substituents have a more planar alignment with the main fluorophores in their ground states but twist out of the main fragment plane upon excitation. The opposite trend is found in our case study.

**3.2. Extending Stokes Shift Structure–Property Relationships to Other Fluorophore Chemical Families.** The “rotating” substituents that induce large Stokes shifts are present not only in coumarins but also in other chemical

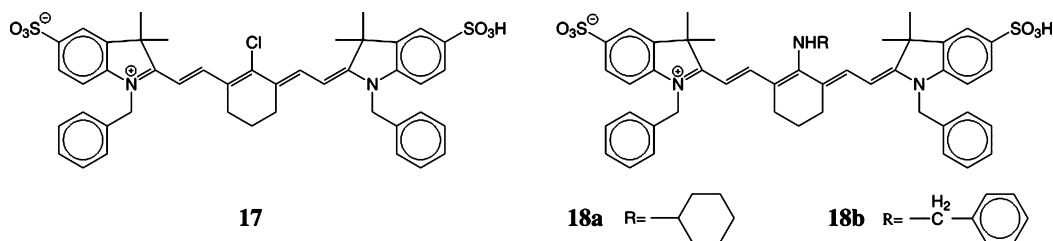
families, such as BODIPY dyes,<sup>32,75–77</sup> heptamethine cyanine dyes,<sup>31</sup> and stilbene derivatives.<sup>78</sup>

**3.2.1. Stokes Shift Trends in BODIPY Dyes.** Selected fluorophores from the BODIPY family (Scheme 4), with substituents at the 2/6- and/or the 8-positions of the core BODIPY fragment (11), are reviewed and analyzed herein. These substituents possess varied electron-donating capabilities and a different extent of rotations upon optical excitation.

We first compare the molecular structures and properties of 12 and 13 (Scheme 4). In 12, the thienyl group at the 8-position is surrounded by two hydrogen atoms attached at the 1- and 7-positions. Due to the relatively modest steric hindrance effect, the dihedral angle,  $\varphi$ , between the thienyl substituent and the BODIPY framework is only 46°, and this substituent is allowed to rotate by 43° during the excited state geometry relaxation, resulting in a large Stokes shift of 100 nm.<sup>32,76</sup> In contrast, by replacing these two hydrogen atoms with two methyl groups at the 1- and 7-positions to generate 13, the contracted space around the 8-position thienyl substituent forces it to twist in its ground state, resulting in a large  $\varphi$  of 90°. This substituent is kept almost completely rigid owing to its neighboring methyl groups and cannot rotate in the excited state.<sup>32,80</sup> Moreover, this vertical alignment essentially isolates the thienyl substitute from the  $\pi$ -conjugated network in the BODIPY framework. Thus the thienyl substitute has very little influence on the optoelectronic properties of 13, resulting in a small Stokes shift of only 11 nm.<sup>32</sup>

We then move our attention to the differences among 14–16, where similar substituents are attached at the 2- and 6-positions (Scheme 4). The thienyl substituents have much larger contributions to the HOMO and LUMO of 14 than the phenyl substituent does in 15 (Figure 8).<sup>32</sup> Consequently, in their excited states, the rotation of the thienyl unit is greater

## Scheme 5. Molecular Structures of Heptamethine Cyanine Dyes, 17, 18a, and 18b



than that of the phenyl unit, being  $16^\circ$  and  $13^\circ$ , respectively.<sup>32</sup> An even more significant difference lies in the impact on their energy levels. For example, the substituent rotations at the 2- and 6-positions in **14** have induced an energy bandgap reduction by 0.49 eV, cf. 0.17 eV in **15**.<sup>32</sup> Consequently, the Stokes shifts of these two compounds are apparently different, measured to be 79 and 26 nm in toluene, respectively.<sup>32</sup>

The Stokes shift of **15** can be enhanced by a subtle molecular modification. We notice that the key difference between **14** and **15** concerns the electron-donating properties of the substituents at the 2- and 6-positions; i.e., the phenyl substituents in **15** are less electron-donating compared to the thienyl units in **14**. To increase the electron-donating power of the phenyl unit, one may add a dimethyl-amino group at the *para*-position, generating **16**. This modification extends the  $\pi$ -conjugation to the phenyl rings in **16**, which, in turn, greatly boosts the contribution of the phenyl rings to the frontier molecular orbitals (Figure 8). We have thus predicted that **16** and related compounds possess considerably larger Stokes shifts, in comparison to **15**. Indeed, a subsequent finding of research by Zhang shows that **16** exhibits a large Stokes shift of 99 nm in both toluene and dichloromethane.<sup>77</sup> Moreover, Martin et al. have also synthesized another similar BODIPY fluorophore, which is **16** substituted with a naphthyridine acceptor site at the 8-position. This new fluorophore exhibits a substantially large Stokes shift of 167 nm in dichloromethane.<sup>75</sup>

### 3.2.2. Stokes Shift Trends in Heptamethine Cyanine Dyes.

A further assessment of the transformative nature of Stokes shift structure–property relationships has been undertaken on the cyanine dyes (Scheme 5). Peng et al. have attached substituents to the  $\pi$ -bridge of a parent heptamethine cyanine dye, **17**, forming two new dyes, **18a** and **18b** (Scheme 5).<sup>31</sup> These two new dyes have significantly larger Stokes shifts,  $\sim 150$  nm, in comparison to 20 nm in their parent dye. The great increase in the Stokes shifts has been attributed the “ICT” state of the new dyes.<sup>31</sup>

The molecular origin of this “ICT” state is actually linked to substituent rotation upon the excitation of **18a** and **18b**. Because of their steric bulk, these substituents are forced to bend out of the molecular plane of the core chemical fragment in their ground state, as suggested by our DFT calculations (Figure 9). These associated TD-DFT calculations also show that the first excited state of **18a** is dominated by a HOMO-1  $\rightarrow$  LUMO transition. During this transition, the electron density around the nitrogen atom in the middle of the  $\pi$ -bridge reveals a significant change. The changing bond character drives the rotation of the  $-\text{NHR}$  substituent toward a more planar alignment with respect to the core molecular fragment, as confirmed by experiments.<sup>31</sup> Such rotations result in significant geometric changes in the excited state of **18a** and **18b**, causing their large Stokes shifts.

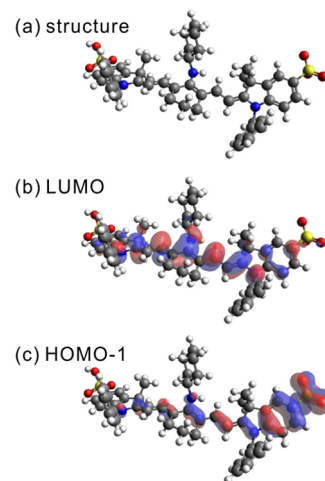


Figure 9. Theoretically optimized molecular structure of **18a** and its LUMO and HOMO-1 (red, positive; blue, negative; isovalue: 0.02).

**3.2.3. Stokes Shift Trends in Stilbene Derivatives.** Finally, we extend this comparison to the popular stilbene dyes. Stilbene (*trans*), **19**, has a very planar structure (Figure 10).

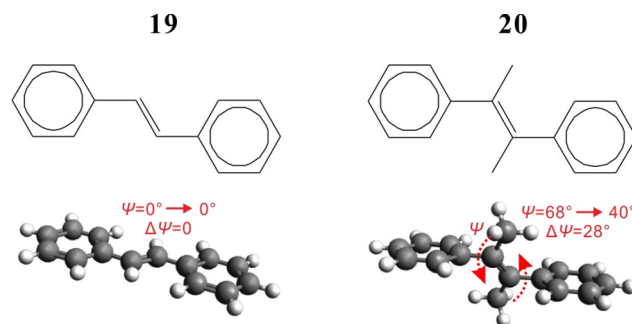


Figure 10. Molecular structures of **19** and **20** and their theoretically optimized geometries in the ground states. According to our DFT/TD-DFT calculations, the dihedral angle between the methyl group and the benzene ring,  $\psi$ , decreases from  $68^\circ$  in the ground state to  $40^\circ$  upon optical excitation in **20**, while the molecular structure of **19** remains flat both in the ground and excited states.

Upon excitation, its structural change is minimal. The RMS of its cumulative atomic displacements is only 0.040 Å. Fischer et al. added two methyl groups onto the stilbene framework and synthesized a new compound, **20**.<sup>78</sup> The interactions between these two methyl groups and the stilbene framework lead to a twisted structure in **20** (Figure 10). Our DFT calculations show that the dihedral angle between the methyl group and the benzene ring,  $\psi$ , is  $68^\circ$  in the ground state of **20**. Upon excitation, however, the methyl group rotates toward a more planar alignment with the stilbene framework, and  $\psi$  decreases

to 40°. Consequently, the RMS of its cumulative atomic displacements rises to 0.279 Å, and the Stokes shift of **20** is significantly larger than that of **19**, by ~76 nm.<sup>78</sup>

### 3.3. Rotating Substituent: Molecular Design Criteria.

Using the structure–property relationship findings for these four families of dyes, we can now propose a few criteria for the molecular design of fluorophores with large Stokes shift via judicious incorporation of rotating chemical substituents.

(a). *Choice of Substituents.* The rotation of substituents upon optical excitation is driven by the increasing strength of the resonance effect. To enhance the resonance effect and produce a large rotation upon photoexcitation, the substituent should have a strong tendency to participate in the  $\pi$ -conjugated network of the main fluorophore. Typical substituents meeting this criteria include (but are not limited to) amino groups and subconjugated systems which are capable of forming conjugated pathways with the main fluorophores (i.e., –CHO, –COCH<sub>3</sub>, –COOH, –C<sub>6</sub>H<sub>5</sub>, and thiophene).

(b). *Steric Hindrance Effect.* There exists an optimal range in the extent of steric hindrance effects to achieve a large Stokes shift. A reasonably strong steric hindrance is required to consume a large amount of torsional work during the substituent rotation, such that a large Stokes shift is afforded. However, an overbearance of steric hindrance effects can completely prevent the substituent rotation, leading to a small Stokes shift.

(c). *Involvement in the Frontier Molecular Orbitals.* For the rotating substituent to produce an observable effect on the optoelectronic properties of a compound, it must demonstrate a significant level of charge transfer between the molecular orbitals that are associated with the S<sub>0</sub> → S<sub>1</sub> transition. These molecular orbitals are typically, but not necessarily, HOMO and LUMO. The active participation of the substituent in this orbital charge transfer has a 2-fold interlinked impact on the substituent effect. First, a large change in electron density (or essentially the changing bonding character) of the substituent drives its rotation in the excited state. Second, to introduce considerable changes to the energy levels of the S<sub>0</sub> and S<sub>1</sub> states, the substituent must present a large amount of charge in the related molecular orbitals.

## CONCLUSION

Attaching the same chemical substituent at different positions in the coumarin framework leads to substantially different optoelectronic properties. For example, attaching a bulky electron-withdrawing group at the 3-position results in a larger red shift in its UV–vis absorption spectra by ~15 nm and an approximately doubled molar extinction coefficient than at the 4-position; attaching this substituent at the 4-position causes a far larger Stokes shift by ~80 nm than at the 3-position.

The molecular origin of these substituent positional effects has been investigated both through empirical HOSE and BLA analysis and theoretical DFT/TD-DFT calculations. It is found that the 3-position accommodates more space which allows a relatively planar alignment of the substituent within the coumarin framework. This alignment results in more significant  $\pi$ -electron delocalization in the conjugated system and leads to a larger red shift in its UV–vis absorption spectra. Furthermore, the 3-position substituent aligns more closely with the ICT direction in the coumarin fragment. It enhances the transition dipole moment more effectively and brings about a higher molar extinction coefficient in its first absorption band. In contrast, owing to stronger steric hindrance effects, the

otherwise analogous 4-position-substituted coumarin is forced to bend out of the molecular plane; its electron-withdrawing effects are thus limited. Nevertheless, this substituent rotates toward a more planar arrangement with respect to the core coumarin framework during the geometry relaxation in its excited state. The torsional work associated with this rotation is responsible for its very large Stokes shift of ~130 nm.

Incorporating a chemical substituent which rotates in the excited state is shown to be an effective method to enlarge the Stokes shift, not only in coumarins but also in other types of fluorophores, such as BODIPY, cyanine, and stilbene dyes. The associated structure–property relationships that determine the Stokes shift in these dye families are used to propose molecular design criteria that enable the prediction of Stokes shifts in fluorophores. The key criteria are: a judicious choice of substituents, an appropriate control of the associated steric hindrance effects, and the active involvement of the substituents in the frontier molecular orbitals of fluorophores. On the basis of this understanding, we have shown how this can lead to the successful predictions of BODIPY fluorophores with large Stokes shifts.

In general terms, we have shown that a proper consideration of the three-dimensional nature of steric hindrance effects requires the assistance of computational chemistry, as does a proper consideration of their impact on the frontier molecular orbitals. A closer link between chemical synthesis and computational analysis is thus expected in the effective design of new fluorophores with rotating substituents.

By understanding relationships between fluorophore structures and their optoelectronic properties in the way that we have presented, one gains the ability to tune the optoelectronic properties of dyes with minimal changes in its molecular size. We believe that the realization of such fundamental knowledge will be very helpful for the rational molecular engineering of better-performing fluorophores. One limitation of this study, however, is that the substituent (positional) effect on the quantum efficiencies of fluorophores, and its diverse impacts (other than on substituent rotations), such as on the tendency to TICT and the extent of ICT upon the excitation of organic fluorophores, cannot be addressed. However, methods by which one can factor in quantum efficiencies are the subject of the future work.

## AUTHOR INFORMATION

### Corresponding Author

\*E-mail: zcxu@dicp.ac.cn. Tel.: +86-411-84379648. Fax: +86-411-84379648 (Z.X.). E-mail: jmc61@cam.ac.uk. Tel.: +44 (0) 1223-337470. Fax: +44 (0)1223-373536. (J.M.C.)

### Notes

The authors declare no competing financial interest.

## ACKNOWLEDGMENTS

The authors would like to acknowledge the use of the EPSRC UK National Service for Computational Chemistry Software (NSCCS) at Imperial College London in carrying out this work. XL is indebted to the Singapore Economic Development Board for a Clean Energy Scholarship. ZX is supported by the National Natural Science Foundation of China (21276251), Ministry of Human Resources and Social Security of PRC, the 100 Talents Program funded by Chinese Academy of Sciences, State Key Laboratory of Fine Chemicals of China (KF1105). JMC thanks the Royal Society for a University Research

Fellowship, the University of New Brunswick (UNB), Canada, for The UNB Vice-Chancellor's Research Chair, and NSERC for the Discovery Grant, 355708.

## REFERENCES

- (1) Lavis, L. D.; Raines, R. T. Bright Ideas for Chemical Biology. *ACS Chem. Biol.* **2008**, *3*, 142–155.
- (2) Que, E. L.; Domaille, D. W.; Chang, C. J. Metals in Neurobiology: Probing Their Chemistry and Biology with Molecular Imaging. *Chem. Rev.* **2008**, *108*, 1517–1549.
- (3) Ueno, T.; Nagano, T. Fluorescent Probes for Sensing and Imaging. *Nat. Methods* **2011**, *8*, 642–645.
- (4) Gonçalves, M. S. T. Fluorescent Labeling of Biomolecules with Organic Probes. *Chem. Rev.* **2009**, *109*, 190–212.
- (5) Luo, S.; Zhang, E.; Su, Y.; Cheng, T.; Shi, C. A Review of NIR Dyes in Cancer Targeting and Imaging. *Biomaterials* **2011**, *32*, 7127–7138.
- (6) Urano, Y.; Asanuma, D.; Hama, Y.; Koyama, Y.; Barrett, T.; Kamiya, M.; Nagano, T.; Watanabe, T.; Hasegawa, A.; Choyke, P. L. Selective Molecular Imaging of Viable Cancer Cells with pH-Activatable Fluorescence Probes. *Nat. Med.* **2008**, *15*, 104–109.
- (7) Schäferling, M. The Art of Fluorescence Imaging with Chemical Sensors. *Angew. Chem., Int. Ed.* **2012**, *51*, 3532–3554.
- (8) Köhler, A.; Wilson, J. S.; Friend, R. H. Fluorescence and Phosphorescence in Organic Materials. *Adv. Eng. Mater.* **2002**, *4*, 453–459.
- (9) O'Regan, B.; Grätzel, M. A Low-Cost, High-Efficiency Solar Cell Based on Dye-Sensitized Colloidal TiO<sub>2</sub> Films. *Nature* **1991**, *353*, 737–740.
- (10) Hagfeldt, A.; Boschloo, G.; Sun, L.; Kloo, L.; Pettersson, H. Dye-Sensitized Solar Cells. *Chem. Rev.* **2010**, *110*, 6595–6663.
- (11) Frangioni, J. V. In Vivo Near-Infrared Fluorescence Imaging. *Curr. Opin. Chem. Biol.* **2003**, *7*, 626–634.
- (12) Lakowicz, J. R. *Principles of Fluorescence Spectroscopy*; Springer: New York, NY, 2006.
- (13) Beija, M.; Afonso, C. A. M.; Martinho, J. M. G. Synthesis and Applications of Rhodamine Derivatives As Fluorescent Probes. *Chem. Soc. Rev.* **2009**, *38*, 2410–2433.
- (14) Ulrich, G.; Ziessele, R.; Harriman, A. The Chemistry of Fluorescent BODIPY Dyes: Versatility Unsurpassed. *Angew. Chem., Int. Ed.* **2008**, *47*, 1184–1201.
- (15) Boens, N.; Leen, V.; Dehaen, W. Fluorescent Indicators Based on BODIPY. *Chem. Soc. Rev.* **2012**, *41*, 1130–1172.
- (16) Loudet, A.; Burgess, K. BODIPY Dyes and Their Derivatives: Syntheses and Spectroscopic Properties. *Chem. Rev.* **2007**, *107*, 4891–4932.
- (17) Xiao, Y.; Liu, F.; Qian, X.; Cui, J. A New Class of Long-wavelength Fluorophores: Strong Red Fluorescence, Convenient Synthesis and Easy Derivation. *Chem. Commun.* **2005**, 239–241.
- (18) Wu, L.; Burgess, K. Syntheses of Highly Fluorescent GFP-Chromophore Analogues. *J. Am. Chem. Soc.* **2008**, *130*, 4089–4096.
- (19) Murale, D. P.; Lee, K. M.; Kim, K.; Churchill, D. G. Facile "One Pot" Route to the Novel Benzazulene-Type Dye Class: Asymmetric, Derivatizable, 5–7–6 Fused Ring Puckered Half Bodipy Design. *Chem. Commun.* **2011**, *47*, 12512–12514.
- (20) Kim, E.; Koh, M.; Ryu, J.; Park, S. B. Combinatorial Discovery of Full-Color-Tunable Emissive Fluorescent Probes Using a Single Core Skeleton, 1,2-Dihydropyrrolo[3,4- $\beta$ ]indolizin-3-one. *J. Am. Chem. Soc.* **2008**, *130*, 12206–12207.
- (21) Kim, E.; Koh, M.; Lim, B. J.; Park, S. B. Emission Wavelength Prediction of a Full-color-tunable Fluorescent Core Skeleton, 9-Aryl-1,2-dihydropyrrolo [3, 4-b] Indolizin-3-one. *J. Am. Chem. Soc.* **2011**, *133*, 6642–6649.
- (22) Yuan, L.; Lin, W.; Yang, Y.; Chen, H. A Unique Class of Near-Infrared Functional Fluorescent Dyes with Carboxylic-Acid-Modulated Fluorescence ON/OFF Switching: Rational Design, Synthesis, Optical Properties, Theoretical Calculations, and Applications for Fluorescence Imaging in Living Animals. *J. Am. Chem. Soc.* **2012**, *134*, 1200–1211.
- (23) Wysocki, L. M.; Lavis, L. D. Advances in the Chemistry of Small Molecule Fluorescent Probes. *Curr. Opin. Chem. Biol.* **2011**, *15*, 752–759.
- (24) Lin, W.; Yuan, L.; Cao, Z.; Feng, Y.; Song, J. Through-Bond Energy Transfer Cassettes with Minimal Spectral Overlap between the Donor Emission and Acceptor Absorption: Coumarin–Rhodamine Dyads with Large Pseudo-Stokes Shifts and Emission Shifts. *Angew. Chem., Int. Ed.* **2009**, *49*, 375–379.
- (25) Jung, G. *Combinatorial Chemistry*; Wiley: Weinheim, Germany, 1999.
- (26) Kennedy, J. P.; Williams, L.; Bridges, T. M.; Daniels, R. N.; Weaver, D.; Lindsley, C. W. Application of Combinatorial Chemistry Science on Modern Drug Discovery. *J. Comb. Chem.* **2008**, *10*, 345–354.
- (27) Kodadek, T. The Rise, Fall and Reinvention of Combinatorial Chemistry. *Chem. Commun.* **2011**, *47*, 9757–9763.
- (28) Wilson, S.; Czarnik, A. Combinatorial Chemistry, Synthesis and Application. *Eur. J. Med. Chem.* **1997**, *32*, 842–842.
- (29) Doroshenko, A. Physicochemical Principles of the Creation of Highly Efficient Organic Luminophores with Anomalously High Stokes' Shifts. *Theor. Exp. Chem.* **2002**, *38*, 135–155.
- (30) Vollmer, F.; Rettig, W.; Birckner, E. Photochemical Mechanisms Producing Large Fluorescence Stokes Shifts. *J. Fluoresc.* **1994**, *4*, 65–69.
- (31) Peng, X.; Song, F.; Lu, E.; Wang, Y.; Zhou, W.; Fan, J.; Gao, Y. Heptamethine Cyanine Dyes with a Large Stokes Shift and Strong Fluorescence: A Paradigm for Excited-State Intramolecular Charge Transfer. *J. Am. Chem. Soc.* **2005**, *127*, 4170–4171.
- (32) Chen, Y.; Zhao, J.; Guo, H.; Xie, L. Geometry Relaxation-Induced Large Stokes Shift in Red-Emitting Borondipyrromethenes (BODIPY) and Applications in Fluorescent Thiol Probes. *J. Org. Chem.* **2012**, *77*, 2192–2206.
- (33) Krygowski, T. M.; Anulewicz, R.; Kruszewski, J. Crystallographic Studies and Physicochemical Properties of  $\pi$ -electron Compounds. III. Stabilization Energy and the Kekulé Structure Contributions Derived from Experimental Bond Lengths. *Acta Crystallogr., Sect. B: Struct. Sci.* **1983**, *39*, 732–739.
- (34) Gorman, C. B.; Marder, S. R. An Investigation of the Interrelationships Between Linear and Nonlinear Polarizabilities and Bond-length Alternation in Conjugated Organic Molecules. *Proc. Natl. Acad. Sci. U.S.A.* **1993**, *90*, 11297–11301.
- (35) Marder, S. R.; Gorman, C. B.; Tiemann, B. G.; Perry, J. W.; Bourhill, G.; Mansour, K. Relation Between Bond-Length Alternation and Second Electronic Hyperpolarizability of Conjugated Organic Molecules. *Science* **1993**, *261*, 186–189.
- (36) Marder, S. R.; Gorman, C. B.; Meyers, F.; Perry, J. W.; Bourhill, G.; Brédas, J. L.; Pierce, B. M. A Unified Description of Linear and Nonlinear Polarization in Organic Polymethine Dyes. *Science* **1994**, *265*, 632–635.
- (37) Frisch, M. J.; Trucks, G. W.; Schlegel, H. B.; Scuseria, G. E.; Robb, M. A.; Cheeseman, J. R.; Scalmani, G.; Barone, V.; Mennucci, B.; Petersson, G. A.; et al. *Gaussian 09*; Gaussian Inc.: Wallingford, CT, 2009.
- (38) Stephens, P. J.; Devlin, F. J.; Chabalowski, C. F.; Frisch, M. J. Ab Initio Calculation of Vibrational Absorption and Circular Dichroism Spectra Using Density Functional Fields. *J. Phys. Chem.* **1994**, *98*, 11623–11627.
- (39) Becke, A. D. Density-Functional Thermochemistry. III. The Role of Exact Exchange. *J. Chem. Phys.* **1993**, *98*, 5648–5652.
- (40) Lee, C.; Yang, W.; Parr, R. G. Development of the Colle–Salvetti Correlation-Energy Formula into a Functional of the Electron Density. *Phys. Rev. B* **1988**, *37*, 785–789.
- (41) Rassolov, V. A.; Ratner, M. A.; Pople, J. A.; Redfern, P. C.; Curtiss, L. A. 6-31G\* Basis Set for Third-Row Atoms. *J. Comput. Chem.* **2001**, *22*, 976–984.
- (42) Chipman, D. M. Reaction Field Treatment of Charge Penetration. *J. Chem. Phys.* **2000**, *112*, 5558–5565.

- (43) Miertus, S.; Scrocco, E.; Tomasi, J. Electrostatic Interaction of a Solute with a Continuum. A Direct Utilization of Ab Initio Molecular Potentials for the Prediction of Solvent Effects. *Chem. Phys.* **1981**, *55*, 117–129.
- (44) Yanai, T.; Tew, D. P.; Handy, N. C. A New Hybrid Exchange-Correlation Functional Using the Coulomb-attenuating Method (CAM-B3LYP). *Chem. Phys. Lett.* **2004**, *393*, 51–57.
- (45) Reynolds, G.; Drexhage, K. New Coumarin Dyes with Rigidized Structure for Flashlamp-pumped Dye Lasers. *Opt. Commun.* **1975**, *13*, 222–225.
- (46) Liu, X.; Cole, J. M.; Waddell, P. G.; Lin, T.-C.; Radia, J.; Zeidler, A. Molecular Origins of Optoelectronic Properties in Coumarin Dyes: Toward Designer Solar Cell and Laser Applications. *J. Phys. Chem. A* **2012**, *116*, 727–737.
- (47) Liu, X.; Cole, J. M.; Waddell, P. G.; Lin, T.-C.; McKechnie, S. The Molecular Origins of Optoelectronic Properties in Coumarins 343, 314T, 445 and 522B. *J. Phys. Chem. C* **2013**, *117*, 14130–14141.
- (48) Wu, W.; Cao, Z.; Zhao, Y. Theoretical Studies on Absorption, Emission, and Resonance Raman Spectra of Coumarin 343 Isomers. *J. Chem. Phys.* **2012**, *136*, 114305.
- (49) Cave, R. J.; Burke, K.; Castner, E. W. Theoretical Investigation of the Ground and Excited States of Coumarin 151 and Coumarin 120. *J. Phys. Chem. A* **2002**, *106*, 9294–9305.
- (50) Cave, R. J.; Castner, E. W. Time-Dependent Density Functional Theory Investigation of the Ground and Excited States of Coumarins 102, 152, 153, and 343. *J. Phys. Chem. A* **2002**, *106*, 12117–12123.
- (51) Liu, X.; Cole, J. M.; Waddell, P. G.; Lin, T.-C. Molecular Origins of Commercial Laser Dye Functionality in Azacoumarins and 2-quinolones: LD 425, LD 489 and LD 473. *Acta Crystallogr., Sect. B: Struct. Sci.* **2011**, *67*, 560–568.
- (52) Fletcher, A.; Bliss, D. Laser Dye Stability. Part 5. *Appl. Phys. A: Mater. Sci. Process.* **1978**, *16*, 289–295.
- (53) Reszka, P.; Schulz, R.; Methling, K.; Lalk, M.; Bednarski, P. J. Synthesis, Enzymatic Evaluation, and Docking Studies of Fluorogenic Caspase 8 Tetrapeptide Substrates. *ChemMedChem* **2010**, *5*, 103–117.
- (54) Besson, T.; Coudert, G.; Guillaumet, G. Synthesis and Fluorescent Properties of Some Heterobifunctional and Rigidized 7-Aminocoumarins. *J. Heterocycl. Chem.* **2009**, *28*, 1517–1523.
- (55) Fletcher, A. N.; Bliss, D. E.; Kauffman, J. M. Lasing and Fluorescent Characteristics of Nine, New, Flashlamp-pumpable, Coumarin Dyes in Ethanol and Ethanol: Water. *Opt. Commun.* **1983**, *47*, 57–61.
- (56) Kauffman, J. M.; Imbesi, S. J.; Aziz, M. A. Synthesis of Julolidine Derivatives. *Org. Prep. Proced. Int.* **2001**, *33*, 603–613.
- (57) Van Gompel, J. A.; Schuster, G. B. Photophysical Behavior of Ester-Substituted Aminocoumarins: a New Twist. *J. Phys. Chem.* **1989**, *93*, 1292–1295.
- (58) Yee, D. J.; Balsanek, V.; Sames, D. Ligands for Aldoketoreductases. WO Patent WO/2006/023,821, March 02, 2006.
- (59) Higashiguchi, K.; Matsuda, K.; Asano, Y.; Murakami, A.; Nakamura, S.; Irie, M. Photochromism of Dithienylethenes Containing Fluorinated Thiophene Rings. *Eur. J. Org. Chem.* **2005**, *2005*, 91–97.
- (60) Roncali, J. Molecular Engineering of the Band Gap of  $\pi$ -Conjugated Systems: Facing Technological Applications. *Macromol. Rapid Commun.* **2007**, *28*, 1761–1775.
- (61) Dean, J. A. *Lange's Handbook of Chemistry*; McGraw-Hill: New York, NY, 1999.
- (62) Jacquemin, D.; Mennucci, B.; Adamo, C. Excited-State Calculations with TD-DFT: from Benchmarks to Simulations in Complex Environments. *Phys. Chem. Chem. Phys.* **2011**, *13*, 16987–16998.
- (63) Richard, R. M.; Herbert, J. M. Time-Dependent Density-Functional Description of the 1 La State in Polycyclic Aromatic Hydrocarbons: Charge-Transfer Character in Disguise? *J. Chem. Theory Comput.* **2011**, *7*, 1296–1306.
- (64) Jacquemin, D.; Adamo, C. Bond Length Alternation of Conjugated Oligomers: Wave Function and DFT Benchmarks. *J. Chem. Theory Comput.* **2010**, *7*, 369–376.
- (65) Jacquemin, D.; Wathelot, V.; Perpète, E. A.; Adamo, C. Extensive TD-DFT Benchmark: Singlet-Excited States of Organic Molecules. *J. Chem. Theory Comput.* **2009**, *5*, 2420–2435.
- (66) Manzhos, S.; Segawa, H.; Yamashita, K. Computational Dye Design by Changing the Conjugation Order: Failure of LR-TDDFT to Predict Relative Excitation Energies in Organic Dyes Differing by the Position of the Methine Unit. *Chem. Phys. Lett.* **2012**, *527*, 51–56.
- (67) Turro, N. J.; Ramamurthy, V.; Scaiano, J. *Modern Molecular Photochemistry of Organic Molecules*; University Science Books: CA, USA, 2010.
- (68) Pavlopoulos, T. Prediction of Laser Action Properties of Organic Dyes from Their Structure and the Polarization Characteristics of Their Electronic Transitions. *IEEE J. Quantum Elect.* **1973**, *9*, 510–516.
- (69) Peach, M. J. G.; Benfield, P.; Helgaker, T.; Tozer, D. J. Excitation Energies in Density Functional Theory: an Evaluation and a Diagnostic Test. *J. Chem. Phys.* **2008**, *128*, 044118.
- (70) Moog, R. S.; Kim, D. D.; Oberle, J. J.; Ostrowski, S. G. Solvent Effects on Electronic Transitions of Highly Dipolar Dyes: a Comparison of Three Approaches. *J. Phys. Chem. A* **2004**, *108*, 9294–9301.
- (71) Liu, X.; Cole, J. M.; Low, K. S. Solvent Effects on the UV-vis Absorption and Emission of Optoelectronic Coumarins: a Comparison of Three Empirical Solvatochromic Models. *J. Phys. Chem. C* **2013**, *117*, 14731–14741.
- (72) Suzuki, H. *Electronic Absorption Spectra and Geometry of Organic Molecules: An Application of Molecular Orbital Theory*; Academic Press: New York, NY, 1967.
- (73) Rettig, W. Charge Separation in Excited States of Decoupled Systems—TICT Compounds and Implications Regarding the Development of New Laser Dyes and the Primary Process of Vision and Photosynthesis. *Angew. Chem., Int. Ed.* **1986**, *25*, 971–988.
- (74) Grabowski, Z. R.; Rotkiewicz, K.; Rettig, W. Structural Changes Accompanying Intramolecular Electron Transfer: Focus on Twisted Intramolecular Charge-Transfer States and Structures. *Chem. Rev.* **2003**, *103*, 3899–4032.
- (75) Martin, A.; Long, C.; Forster, R. J.; Keyes, T. E. Near IR Emitting BODIPY Fluorophores with Mega-Stokes Shifts. *Chem. Commun.* **2012**, *48*, 5617–5619.
- (76) Kim, K.; Jo, C.; Easwaramoorthi, S.; Sung, J.; Kim, D. H.; Churchill, D. G. Crystallographic, Photophysical, NMR Spectroscopic and Reactivity Manifestations of the “8-Heteroaryl Effect” in 4,4-Difluoro-8-(C<sub>4</sub>H<sub>3</sub>X)-4-bora-3a,4-a-diaza-s-indacene (X = O, S, Se)(BODIPY) Systems. *Inorg. Chem.* **2010**, *49*, 4881–4894.
- (77) Zhang, D. The Research on Synthetic Methodology and Spectral Properties Based on BODIPY Dyes. Ph.D. Dissertation, Dalian University of Technology, Dalian, China, 2010.
- (78) Fischer, G.; Seger, G.; Muszkat, K. A.; Fischer, E. Emissions of Sterically Hindered Stilbene Derivatives and Related Compounds. Part IV. Large Conformational Differences Between Ground and Excited States of Sterically Hindered Stilbenes: Implications Regarding Stokes Shifts and Viscosity or Temperature Dependence of Fluorescence Yields. *J. Chem. Soc., Perkin Trans. 2* **1975**, 1569–1576.
- (79) Jun, T.; Kim, K.; Lee, K. M.; Benniston, A. C.; Churchill, D. G. Meso-thienyl and Furyl Rotor Effects in BF<sub>2</sub>-Chelated Dipyrroin Dyes: Solution Spectroscopic Studies and X-ray Structural Packing Analysis of Isomer and Congener Effects. *J. Coord. Chem.* **2012**, *65*, 4299–4314.
- (80) Kee, H. L.; Kirmaier, C.; Yu, L.; Thamyongkit, P.; Youngblood, W. J.; Calder, M. E.; Ramos, L.; Noll, B. C.; Bocian, D. F.; Scheidt, W. R.; Birge, R. R.; Lindsey, J. S.; Holten, D. Structural Control of the Photodynamics of Boron–Dipyrroin Complexes. *J. Phys. Chem. B* **2005**, *109*, 20433–20443.